ChemPubSoc Europe

DOI: 10.1002/cssc.201600290

CHEMSUSCHEM Communications

Electrocatalytic Hydrogenation of Oxygenates using Earth-Abundant Transition-Metal Nanoparticles under Mild Conditions

Kyler J. Carroll[+],[a] Thomas Burger[+],[a, b] Lukas Langenegger,[a, c] Steven Chavez,[a] Sean T. Hunt,[a] Yuriy Román-Leshkov,[a] and Fikile R. Brushett*[a]

Electrocatalytic hydrogenation (ECH) is a sustainable pathway for the synthesis of value-added organic compounds, provided affordable catalysts with high activity, selectivity and durability are developed. Here, we synthesize Cu/C, Ni/C, and CuNi/C nanoparticles and compare their performance to Pt/C, Ru/C, PtRu/C for the ECH of hydroxyacetone, a bio-derived feedstock surrogate containing a carbonyl and a hydroxyl functional group. The non-precious metal electrocatalysts show promising conversion-time behavior, product selectivities, and Faradaic efficiencies. Ni/C forms propylene glycol with a selectivity of 89% (at 80% conversion), while Cu/C catalyzes ECH (52% selectivity) and hydrodeoxygenation (HDO, 48% selectivity, accounting for evaporation). CuNi/C shows increased turnover frequencies but reduced ECH selectivity (80% at 80% conversion) as compared to the Ni/C catalyst. Importantly, stability studies show that the non-precious metal catalysts do not leach at operating conditions.

Liquid-phase heterogeneous catalytic hydrogenation (CH) is an important pathway for the reduction of hydrogen-deficient biomass compounds.[1–4] Liquid-phase hydrogenation reactions require high pressures of hydrogen gas (>30 bar) to attain appropriate dissolution of hydrogen. Furthermore, reaction rates acceptable for practical applications can only be obtained by using late-transition-metal catalysts.[2,5] Recent efforts to overcome these challenges have largely focused on replacing precious metals with earth-abundant elements or using different pathways, such as transfer hydrogenation with hydrogen donors.[6,7] Electrochemistry provides an alternative avenue to perform chemical transformations and can be carried out at low temperatures and atmospheric pressures. Additionally, utilizing water as the donor of surface-bound hydrogen eliminates the need for an external hydrogen source. Electrochemical hydrogenation (ECH) is ideal for biomass processing, because it can be readily deployed in small biorefineries. Moreover, electrons can be harnessed directly from available renewable electricity generators, such as wind turbines or solar photovoltaics.

In this work, the performance of carbon-supported non-precious metal nanoparticles is investigated and compared to conventional carbon-supported precious metal nanoparticles. The performance of these catalysts is assessed through the ECH of hydroxyacetone, a model compound containing both keto and hydroxyl functional groups. Indeed, carbonyl functional groups are commonly found in the presence of hydroxyl moieties in several biomass-derived oxygenates, such as hexoses, pentoses, trioses, and hydroxymethylfurfural (HMF). As such, understanding their reactivity pathways (e.g., hydrogenation vs. hydrogenolysis) is important to modulate product selectivity. Here, copper and nickel nanoparticles are studied for the selective ECH of hydroxyacetone to propylene glycol at a mild applied potential (−1.5 V vs. Ag/AgCl) and solution acidity (pH 2).

One possible pathway via which the ECH reaction could proceed is depicted in Figure 1. During ECH over a catalytic surface, water-derived hydrogen atoms adsorbed on the surface (M-H_{ads}) react with an adsorbed organic molecule (M-X=Y_{ads}) to generate a reduced species (HX-YH). However, low pH values also promote the undesired hydrogen evolution reaction (HER), wherein two proton species combine to generate a hydrogen molecule (H_2). The mechanisms for HER are well-understood and are known to occur via competing Volmer–Heyrovsky and Volmer–Tafel reaction pathways.[8] The Volmer step is pH-dependent and involves the adsorption of protons to generate surface-bound hydrogen (M-H_{ads}). This step is important for both hydrogen evolution and electrocatalytic hydrogenation or hydrodeoxygenation (HDO) processes. The Heyrovsky and Tafel steps are H_2-desorption processes that consume surface-bound hydrogen and adversely affect the desired ECH/HDO process. While H_{ads}-surface coverage is limited by the number of exposed metal atoms (the limiting factor of the Tafel step), the rate of the Heyrovsky step continues to increase with decreasing pH. Additionally, low pH values shift the half-cell potential to more positive values according to the

[a] Dr. K. J. Carroll,[+] T. Burger,[+] L. Langenegger, S. Chavez, S. T. Hunt, Prof. Y. Román-Leshkov, Prof. F. R. Brushett
Department of Chemical Engineering
Massachusetts Institute of Technology
77 Massachusetts Ave, Cambridge, MA 02139 (USA)
E-mail: brushett@mit.edu

[b] T. Burger[+]
Department of Chemistry
Technical University of Munich
Lichtenbergstraße 4, 85748 Garching (Germany)

[c] L. Langenegger
Institute for Chemical and Bioengineering
ETH Zürich
Vladimir-Prelog-Weg 1, 8093 Zürich (Switzerland)

[+] These authors contributed equally to this work.

Supporting Information and the ORCID identification number(s) for the author(s) of this article can be found under http://dx.doi.org/10.1002/cssc.201600290.

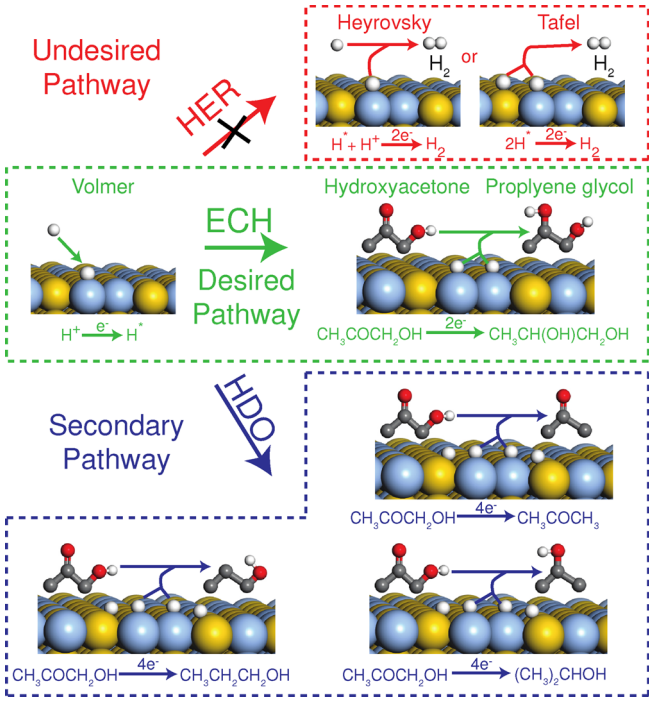

Figure 1. Electrochemical pathways: 1) H_{ads}-generation (Volmer step), 2) H_{ads}-removal by HER (Heyrovsky and Tafel steps, red), selective hydrogenation (green, ECH) or secondary hydrodeoxygenation (blue, HDO) reactions.

Nernst equation, promoting metal leaching. Therefore, acidic conditions, common in bioprocessing, are challenging in terms of both efficiency for ECH/HDO and catalyst stability. Despite its use in the removal of oxygenates, the primary focus of this work is not the HDO reaction, because the HDO process typically requires more electrons than the ECH process.

An efficient catalyst must allow for stabilization of adsorbed hydrogen (H_{ads}) to promote ECH/HDO pathways, while minimizing molecular hydrogen desorption. Recently, Li et al. found ruthenium supported on activated carbon cloth (ACC) to be an active catalyst for ECH and HDO of biomass-derived phenolic compounds.[9] Additionally, ion-exchanged ruthenium catalysts showed higher reactivity than catalysts prepared by incipient wetness impregnation. Those experiments, however, were carried out at a very high applied potential (−7 V vs. Ag/AgCl) and with a precious metal electrocatalyst. Nilges and Schröder reported the HDO of furfural at bulk copper electrodes in acidic media, with high selectivity to methylfurans.[10] In another work, Li et al. introduced bulk nickel electrodes for the selective hydrogenation of furfural to furfuryl alcohol.[11] While previous literature has primarily focused on proof-of-concept demonstrations, systematic studies comparing different catalysts under similar well-defined conditions are lacking. Further, similar to advances made in fuel cell technologies in the early 1990s, while bulk materials serve as a useful platform for initial studies, nanostructured materials are likely to give higher performance and, potentially, to impart new catalytic activities. To this end, we evaluate the performance of a series of carbon-supported precious (platinum, ruthenium, platinum–ruthenium) and non-precious metal (copper, nickel, copper–nickel) nanoparticle catalysts under identical conditions, using the conversion of hydroxyacetone to propylene glycol as a probe reaction.

Figure 2A illustrates the selectivity values obtained towards the different reaction products at ca. 80% hydroxyacetone conversion for various precious and non-precious metal catalysts. For all catalysts, propylene glycol (via ECH) is the favored reaction product, with Ni/C featuring the highest selectivity (89%). Selectivity values of 87% were obtained for Pt/C and PtRu/C, and 81% for Ru/C. The Cu/C catalyst featured the lowest selectivity towards ECH, reaching only ca. 52%. The HDO side reaction yields mainly acetone, 1-propanol, and 2-propanol. For the Cu/C catalyst, selectivities to HDO products reach ca. 48% (when accounting for product evaporation), with acetone as the major product. The observed HDO selectivity of copper is consistent with prior reports for bulk copper electrodes.[10,11] Alloying nickel with copper leads to a decrease in ECH selectivity of ca. 10% as compared to the parent Ni/C catalyst (ca. 89% selectivity towards ECH). In turn, this bimetallic catalyst showed the highest selectivity towards 1-propanol (ca. 1.2%) of all the catalysts tested. The HDO selectivity of the Pt/C and PtRu/C catalysts was much lower than that of the non-precious catalysts, but Ru/C showed a comparatively high selectivity towards acetone. The results suggest that a balance between ECH and HDO selectivity could be achieved through the synthesis of stoichiometrically alloyed nanostructured non-precious catalysts, providing a unique opportunity to selectively target desired reaction products.

As seen in Figure 2B, the ECH selectivity for the Pt/C and Ru/C catalysts is ca. 85–90% at moderate conversions (40–60%). However, at higher conversion the selectivity decreases by 19%, 17%, and 12% for platinum–ruthenium, platinum, and ruthenium, respectively. In contrast, the earth-abundant catalysts show a different behavior. Specifically, the initial selectivities of Ni/C (92%), CuNi/C (90%), and Cu/C (78%) steadily decrease, reaching a global minimum at moderate conversions (25–60%, catalyst-dependent), then increase again slightly (ca. 10–15%), reaching a steady-state without any further decrease in selectivity at high conversions. The minimum in ECH selectivity is directly correlated to the maximum in HDO selectivity. For conversions higher than 80%, Ni/C featured the highest selectivity towards ECH (86–89%). As reported in literature, nickel is also selective for the electrocatalytic hydrogenolysis of benzyl ethers in the form of Raney nickel,[12] and the ECH of furfural.[11] While large variations in ECH/HDO selectivities as a function of conversion percentage is not particularly advantageous, it is worth noting that the Ni/C catalyst shows the lowest loss in ECH selectivity over the entire range of conversions.

Figure 2C illustrates the time-dependent trends in hydroxyacetone conversion obtained for the various electrocatalysts. The figure represents three distinct snapshots over a 300 min range (the full data set can been found in the Supporting Information, Figure S3). The first plot shows that within the first 20 min, the precious metal catalysts have higher reaction rates when compared to the non-precious catalysts. Specifically, PtRu/C generates a conversion of 25% after 15 min, compared

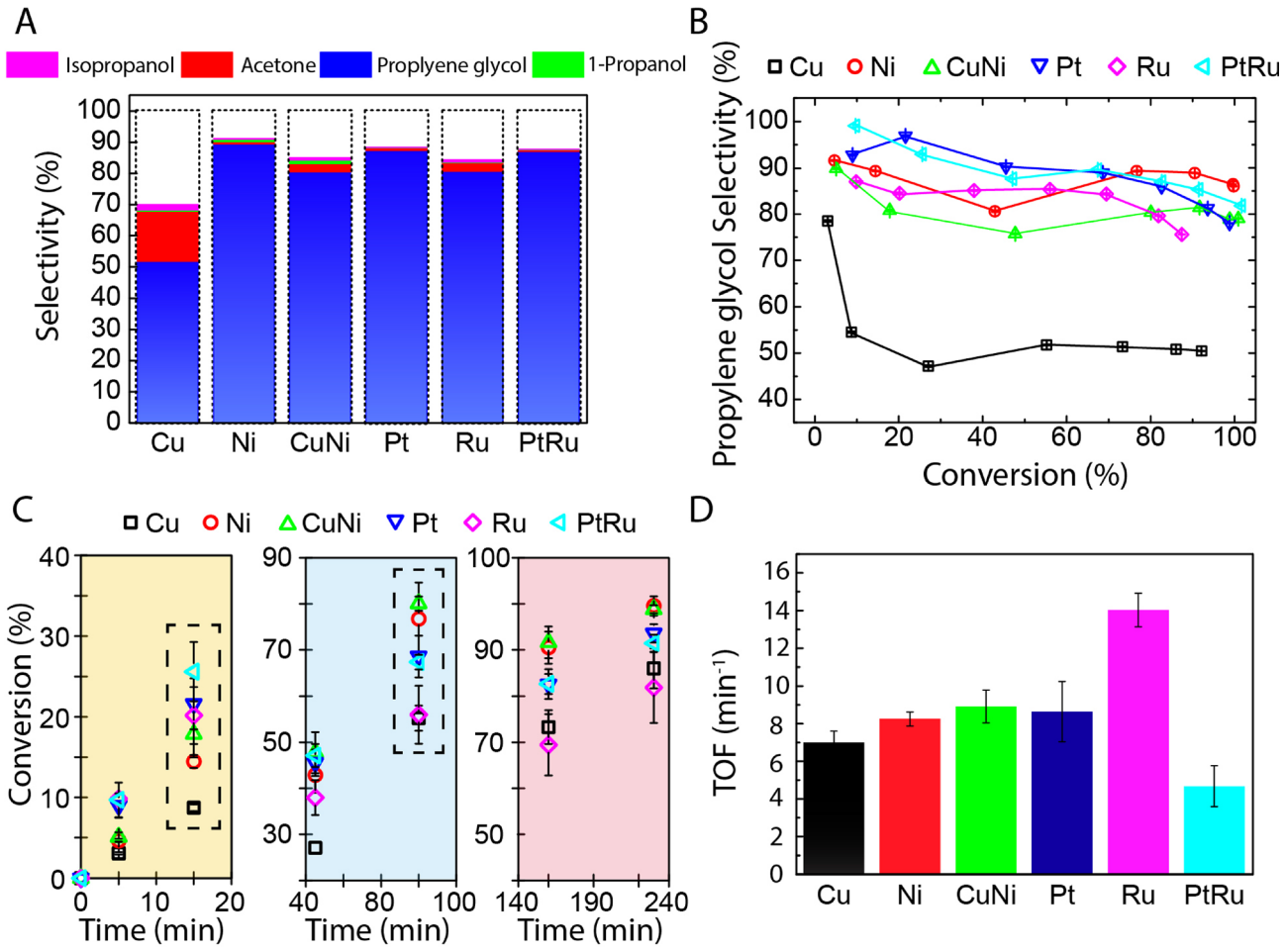

Figure 2. A) Observed selectivity towards different reaction products at 80% conversion of hydroxyacetone (note that the blank space represents unaccounted species), B) selectivities towards propylene glycol (via ECH), C) snapshots of the conversion-time behavior and D) turnover frequencies (TOFs), determined after 5 min, for Cu/C, Ni/C, CuNi/C, Pt/C, Ru/C, and PtRu/C. Measurements were carried out at room temperature and at −1.5 V vs. Ag/AgCl with an initial hydroxyacetone concentration of 50 mM.

to the 15 and 8% conversion values observed for Ni/C and Cu/C. As shown in Figure 2D, a comparison of turnover frequencies (TOFs; defined as molecules converted per surface metal atom per unit time) shows that Pt/C and Ru/C have higher site-normalized initial reaction rates than the non-precious catalysts under conditions free of mass transfer limitations. The highest TOF was obtained for Ru/C (14.0 min^{-1}), with lower TOFs observed for Pt/C (8.6 min^{-1}) and PtRu/C (4.7 min^{-1}). Promisingly, the non-precious catalysts demonstrated TOFs that compared favorably to their precious metal counterparts. Specifically, Ni/C (8.3 min^{-1}) has a higher TOF than Cu/C (7.0 min^{-1}), while CuNi/C (8.9 min^{-1}) was found to be slightly more active than the monometallic representatives. However, a trend starts to appear at ca. 40 min where the reaction rates for Ni/C and CuNi/C increase until roughly 90 min, surpassing the rates observed for the precious metal catalysts. Ultimately, the CuNi/C (ca. 80%) and Ni/C (ca. 78%) outperform all other catalysts, thus indicating that while initially the precious metal catalysts outperform the non-precious metal catalysts, higher conversions can be seen with the non-precious metal catalysts after ca. 60 min. We note that although our data cannot exclude the direct reduction of our substrate with H_2 evolved from the HER reaction, it is unlikely that direct hydrogenation activity would have significant rates under atmospheric conditions.

In general, the initial (maximal) Faradaic efficiencies for the conversion of hydroxyacetone to propylene glycol (via ECH) are modest in the present system: 11% for Cu/C, 17% over Ni/C, 16% for CuNi/C, 20% for Pt/C, and 22% for Ru/C and PtRu/C, but these values are expected to increase with increased oxygenate concentrations as well as improved reactor design and operation modes. Over the electrolysis time of 5 h the Faradaic efficiencies were 3.5% for Cu/C, 5.6% for Ni/C, 4.8% for CuNi/C, 3.0% for Pt/C, 2.9% for Ru/C and 3.1% for PtRu/C. We also note that the cell and the applied potential (−1.5 V vs. Ag/AgCl), which is lower than the hydrogen evolution potential (−0.33 V vs. Ag/AgCl at pH 2) and the hydroxyacetone to propylene glycol reduction potential (0.35 V vs. Ag/AgCl at pH 2), is not designed for efficiency.

During all experiments, constant currents were observed. Assuming a constant number of active species present on the catalyst surface, this implies that the number of species being

reduced, that is, hydroxyacetone through ECH/HDO or protons through HER, does not change. The competition between HER and ECH/HDO becomes apparent in the time-conversion plot shown in Figure 2C (full data set can be found in Supporting Information, Figure S3), where the initially high reaction rates rapidly decrease as the hydroxyacetone concentration gradually depletes. In contrast, this competition is less conversion-dependent for the non-precious metal catalysts. Despite the fact that the initial reaction rates are smaller, their decrease is comparatively lower, resulting in higher ECH/HDO rates over longer durations. The results also indicate that alloying copper and nickel to form the CuNi/C catalyst enhances hydroxyacetone conversion rates over their monometallic counterparts. X-ray diffraction patterns (Supporting Information, Figure S4) and high-resolution microscopy images (Supporting Information, Figure S6) clearly show the formation of a copper–nickel alloy.

In combination with the selectivity trends shown in Figure 2A, we hypothesize that the presence of copper atoms with nickel opens additional reaction pathways, such as HDO to acetone or multistep reductions, resulting in an increase in activity and decrease in ECH selectivity. Synergistic effects between copper and nickel supported on alumina have previously been reported to cause changes in selectivity in furfural hydrogenation that depend on catalyst composition.[13]

In contrast, the diffraction patterns, as well as the microscopy images for PtRu/C catalysts, suggest the formation of a co-dispersion of monometallic nanoparticles with independent reflections for both platinum and ruthenium. The higher TOF observed for the monometallic catalysts within the first 5 min suggests a negative correlation for having both metals co-dispersed over having a bimetallic nanoparticle formulation, and indicates a greater preference of HER over ECH/HDO.

The initial reaction rates (vide supra) were normalized to the number of surface metal atoms, as determined by elemental analysis (through inductively coupled plasma optical emission spectrometry; ICP–OES) and particle size distributions calculated from transmission electron microscopy (TEM) images (see Supporting Information, Figure S7). The as-synthesized non-precious metal particles were generally larger than the precious metal particles (Figure 3A, B, and C). Additionally, the images show the good dispersion of precious metal particles (Figure 3D–F). In contrast to literature reports,[13] smaller particle diameters were found for CuNi/C compared to their monometallic counterparts. The metal loading, particle diameter, and dispersion data for all precious and non-precious catalysts are shown in Table 1.

At 80% conversion, approximately 8% of the initial reactant was unaccounted for based on the experiments using Ni/C (see Figure 2A). We attribute these carbon losses to evaporation of volatile products and to species crossover and oxidation at the anode. Note that isopropanol, acetone, and 1-propanol were found in small concentrations in an ice-water-cooled condensation trap attached to the electrolysis cell, providing evidence of evaporation during the experiment. Experiments carried out using a Cu/C electrode and an online mass spectrometer corroborated gas formation by showing propene, propane, and acetone in the effluent stream (see Supporting Information, Figure S4). In Figure 2A, the unassigned selectivities are proportional to the selectivity of acetone, which is due to increased volatile product evaporation. Furthermore, decomposition reactions on the anode, due to species crossover, yielded acetone, formic acid, and acetic acid. In addition, small amounts of ethanol, as well as ethane, ethylene, and methane formation could be detected in gas chromatography for both precious and non-precious catalysts. Ethanol, ethylene, and ethane have previously been reported as reduction products of acetic acid on Ru/C.[14] However, no methanol could be detected owing to peak overlap with hydroxyacetone during HPLC analysis. Non-decreasing propylene glycol yields suggest that isopropanol and 1-propanol are generated by multiple $2e^-$ steps or a direct $4e^-$ reduction process. Propylene glycol was not reduced in a 2 h control experiment using a concentration of 50 mM and a CuNi/C electrode. Additionally, to account for substrate effects, blank tests carried out with VULCAN carbon resulted in 41.7% conversion after 5 h, suggesting some substrate activity (see Supporting Information, Figure S2).

Stability and deactivation rates are important metrics for catalyst performance. In liquid-phase catalysis, deactivation is mainly a result of a loss in active sites due to leaching, particle sintering, or poisoning. However, in ECH, the application of a sufficient reduction potential, past the formal potential of the metal catalyst, preserves the metal species on the working

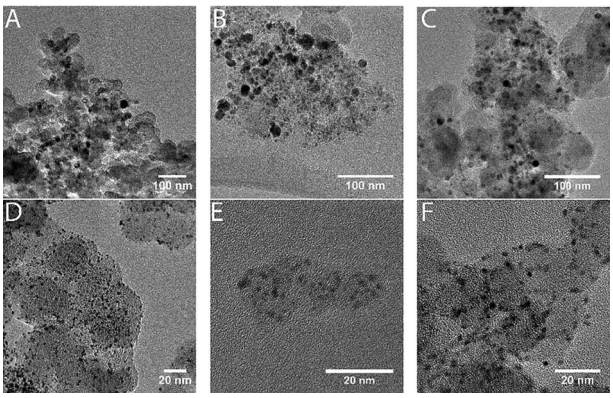

Figure 3. TEM images of Cu/C (A), Ni/C (B), CuNi/C (C), Pt/C (D), Ru/C (E), and PtRu/C (F).

Table 1. Catalyst metal loading, particle diameter, and dispersion for Cu/C, Ni/C, CuNi/C, Pt/C, Ru/C, and PtRu/C.

Sample	Metal loading [%]	Particle diameter [nm]	Dispersion [%]
Cu/C	9.6	8.70	12.0
Ni/C	8.79	6.57	15.4
CuNi/C	4.04 (Cu) 4.64 (Ni)	6.44	15.9
Pt/C	9.64	1.32	85.3
Ru/C	3.28	1.51	85.7
PtRu/C	3.27 (Pt) 8.02 (Ru)	1.44	82.7

electrode, and therefore decreases the leaching rate of metal ions from the nanoparticles. ICP-OES analysis of samples taken from the electrolyte under operating conditions show negligible metal contamination, even after 5 h. However, samples taken after switching to open-circuit potential (OCP) revealed a loss of 4.5% copper and 12.9% nickel on the CuNi/C catalyst after a 5 h reaction. We note that no leaching could be detected for the precious metal catalysts at OCP. X-ray photoelectron spectroscopy (XPS) analyses on CuNi/C, Cu/C, and Ni/C post-reaction (after exposing the electrode to OCP) corroborates the loss of metal ions only for the non-precious catalysts (see Supporting Information, Figure S9). The findings confirm that acid leaching for non-precious metal catalysts does not actually occur under reaction conditions and suggest that increased stability may be realized by maintaining potentials below the metal electrodeposition potential. This can be regarded as another benefit of using ECH for aqueous-phase hydrogenation reactions with non-precious metal catalysts, especially since non-precious metal catalysts suffer from deactivation by active site loss owing to leaching under thermal liquid-phase hydrogenation conditions.[15,16,17] Lastly, post-reaction (5 h) TEM analyses of Ni/C, CuNi/C, and PtRu/C nanoparticles show no increase in mean particle diameter, but do show particle mobility during the reaction. Sintering and coalescence behavior has been seen for gold nanoparticles, however to a much greater degree than that observed in this study.[18]

The performance of earth-abundant metal catalysts in ECH can be further highlighted by normalizing the TOF values to the metal costs as shown in Figure 4A.[19] Due to their lower costs, non-precious metal catalysts outperform platinum-based catalysts by three orders of magnitude. The high ECH/HDO activity of platinum-group metals is diminished by their low availability and prohibitive costs.[19] Catalyst design can contribute to further improving the capability of nickel-based catalysts for ECH. In addition to metal costs, Faradaic efficiency for the electrochemical reduction of oxygenates is an important economic factor.

In Figure 4B, the TOFs are normalized to the observed charges at −1.5 V vs. Ag/AgCl. This serves as a means of comparing the relative ECH efficiencies of each catalyst. Owing to their comparatively high HER activity,[20] platinum-based metals draw higher currents than the non-precious metal catalysts at equivalent hydroxyacetone conversion rates. For constant hydrogen surface coverage at constant pH and number of active sites, the decrease of reactive organic species in solution is competitively compensated for by an increase in HER activity. This is most likely the cause of the strong reaction rate dependence on organic reactant concentration observed for the platinum-group metals in Figure 2A, opposite to non-precious metal catalysts, which comparatively show better performance at higher conversions. This also implies the reduction of the Faradaic efficiency for ECH/HDO with increasing time in batch operation mode for precious metal catalysts. Beside its advantage in process management, continuous operation in this reaction would provide constant Faradaic efficiencies, without active site loss due to leaching being a significant deactivation mechanism.

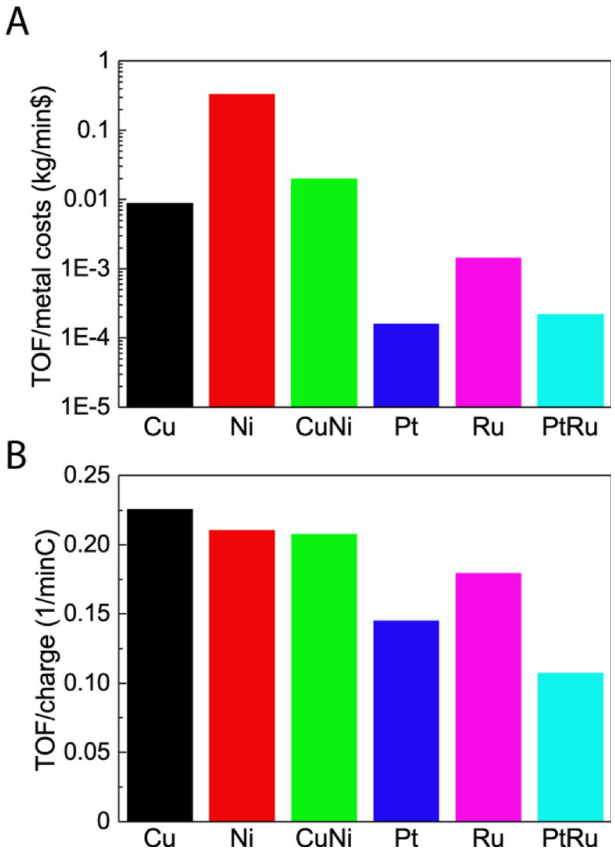

Figure 4. A) Metal cost normalized, and B) charge-normalized turnover frequencies calculated after 5 min at −1.5 V vs. Ag/AgCl at room temperature with an initial concentration of 50 mM hydroxyacetone.

This work compares the performance of precious- and non-precious metal electrocatalysts for the selective electrochemical hydrogenation of hydroxyacetone to propylene glycol. Under sufficient negative working potentials (−1.5 V vs. Ag/AgCl), Ni/C shows the highest ECH selectivity while Cu/C is also selective for a secondary pathway, HDO. By alloying the two non-precious metals, higher hydroxyacetone reduction reaction rates are achieved albeit with slightly diminished propylene glycol selectivity and new product formation. TOF results suggest that Pt/C and Ru/C have higher initial reaction rates in ECH/HDO but, away from initial conditions, where the hydroxyacetone concentration influences the reaction rate, the non-precious metals outperform the precious metal catalysts in terms of substrate conversion. We hypothesize that this behavior is due to the competing HER, which starts to dominate as the organic reactant is depleted, and the interplay between surface-bound hydrogen and local hydroxyacetone concentration. Ni/C outperforms all catalysts in terms of total conversion selectivity for ECH. Higher crustal abundance and lower metal prices make Ni/C an attractive candidate for large-scale electrochemical hydrogenation. Future work will focus on evaluating the performance of these electrocatalysts with molecules (e.g., levulinic acid) featuring carbonyl groups at different locations within the carbon backbone and/or in the presence of other functional groups.

Experimental Section

$Ni(NO_3)_2{\cdot}6(H_2O)$ (Sigma–Aldrich) was used as nickel precursor, $Cu(NO_3)_2{\cdot}3(H_2O)$ (Sigma–Aldrich) and $RuCl_3$ (Sigma–Aldrich) were used as copper and ruthenium precursors, respectively. 10% PtRu/VC (from http://www.fuelcellstore.com; accessed June 2016) and 10% Pt/VC (Sigma–Aldrich) were used as-received.

The catalysts were prepared by incipient wetness impregnation. First, the VULCAN XC72R carbon black (CABOT) support was acid-treated to decrease hydrophobicity and to remove any impurities, by stirring in 6 M HCl for 16 h. After filtrating to pH 5, the retentate was dried at 60 °C overnight. Then, 500 mg were ground using a mortar and pestle for 30 min under dropwise addition of 2.975 mL metal salt solution. The impregnated catalysts were dried in the oven at 60 °C overnight and reduced at 400 °C in a pure hydrogen stream at a flow rate of 0.2 mL min^{-1}. Reduction time was 1 h at a heat ramp of 2 °C min^{-1}.

To improve conductivity and remove impurities, a 26 cm^2 piece of Nafion 117 (N117, Ion Power) was treated using the following procedure: the membrane was first boiled for 1 h in 3% H_2O_2 and subsequently boiled in DI water 3 times, for 30 min each time. The membrane was rinsed with DI water after each boil. The membrane was then boiled in 0.25 M H_2SO_4 for 1 h, and again boiled in DI water 3 times for 30 min each time and rinsed with DI water in-between.

Catalyst powder (10 mg) was dispersed in a mixture of 400 μL of DI water, 400 μL of isopropanol (Sigma–Aldrich), and 6.9 μL of 5% Nafion solution (Liquion, Ion Power). The slurry was sonicated for 10 min and then sprayed onto a gas diffusion layer (GDL, 10 BC, Ion Power), obtaining a coated area of 3.5 cm^2. The air brush (Speedaire) was sonicated and rinsed before spraying each catalyst. Intermediate weighing of the GDL was performed to ensure an overall catalyst mass of 3.5 mg, for a total loading of 1 mg cm^{-2}. With an overall GDL size of 15×45 mm^2, the coated GDL was contacted at the left space using a copper wire of 1 mm diameter. Silver paint (SPI) provided adhesion and small contact resistance. The GDL was covered with Kapton tape (DuPont) on edges, front-, and backside, leaving only the spray-coated areas uncovered. Only the sprayed surface area was exposed to the electrolyte to eliminate contamination of the silver paint and copper wire.

The electrochemical experiments were carried out in an H-cell (see Supporting Information, Figure S1) containing 14 mL of electrolyte in each compartment and separated by the protonated N117 membrane. In all experiments, a gas diffusion electrode (described before) was used as a working electrode, with a platinum coil counter electrode and a Ag/AgCl reference electrode (both BASi). The working and reference electrodes were housed in the same compartment while the counter electrode was placed in the other compartment. Each electrolyte compartment was stirred using a stir-plate at 1600 rpm. To minimize evaporation, both compartments were capped with rubber stoppers. While a needle provided pressure compensation for the anolyte, the catholyte exhaust was led into 14 mL of water to reabsorb any species that left the catholyte. For catalyst screening, prior to experiments, the electrolyte solution was purged with N_2 for 15 min to remove dissolved oxygen. A 0.5 M solution of Na_2SO_4 (>99% purity, anhydrous, Sigma Aldrich) at pH 2 was used as the catholyte while 0.5 M Na_2SO_4 at pH 0.6 was used as the anolyte. Solution pH was adjusted using sulfuric acid (H_2SO_4, 95–98% purity, Sigma–Aldrich). 51.35 μL of hydroxyacetone (95% purity, pH ~3.5, Alfa Aesar) was added to 14.2 mL of catholyte to obtain a 50 mM solution of hydroxyacetone. When not in use, the hydroxyacetone was stored in a lab refrigerator (1–7 °C, Marvel 6FRF). Minimal amounts of hydroxyacetone dimer, formic, and acetic acid were found in the stock and these values did not change across electrocatalyst testing. A Bio-Logic VMP3 potentiostat was used in galvanostatic or potentiostatic mode, depending on the experiment. For catalyst activation, a cyclic voltammogram was taken at a scan rate of 20 mV s^{-1} from −1.5 V to 0 V vs. Ag/AgCl and a subsequent 20 min chronoamperometry at −1.5 V vs. Ag/AgCl were run before electrolysis. Catalyst testing was conducted at a constant potential of −1.5 V (vs. Ag/AgCl) for a total reaction time of 5 h. To compensate for H^+-consumption in the catholyte solution and to maintain a constant pH throughout the reaction, 25 vol% H_2SO_4 was continuously added by a syringe pump (Harvard System) to the catholyte, using a 5 mL syringe (BD). To prevent local pH decrease, a small-diameter hose was placed within the solution, leading to near immediate and uniform proton distribution. The rate of addition varied by experiment. Changes in the electrolyte conductivity and pH were monitored and found to be negligible. Sample volumes taken for high performance liquid chromatography (HPLC, Agilent 1200) were 251.35 μL for the starting concentration, 100 μL for all subsequent samples. Volume loss due to gas evolution was compensated each time before taking the sample by adding DI water. During chronoamperometry, N_2 gas was purged into the catholyte headspace in order to dilute the hydrogen stream and all gas phase products. The exit streams of both electrolyte compartments were fed through an ice bath in order to trap any gas-phase products that formed during the reaction and would otherwise be missed as products from the HPLC analysis. The total reaction time was 5 h with 0.1 mL liquid samples being taken after 5, 15, 45, 100, 160, 230 and 300 min. The solution temperature was monitored before and after the reaction by a thermometer and remained constant at room temperature. All data were collected at least in triplicate. Concentrations were determined by HPLC for liquid-phase reactants, and by gas chromatography (GC, Agilent) for gaseous products.

Additional characterization details can be found in the Supporting Information.

Acknowledgements

The authors acknowledge the contribution of H. Luo, Y. Wang, G. Veith, M. Orella, and O. Hinrichsen. T.B. acknowledges the Ernest-Solvay-Foundation and the Elite Network of Bavaria for financial support. S.H. acknowledges financial support by the National Science Foundation Graduate Student Fellowship and CAREER Award (1122374).

Keywords: electrocatalysis · heterogeneous catalysis · hydrogenation · nickel · renewable resources

[1] Y. Román-Leshkov, C. J. Barrett, Z. Y. Liu, J. A. Dumesic, *Nature* **2007**, *447*, 982–985.
[2] J. Jae, W. Zheng, R. F. Lobo, D. G. Vlachos, *ChemSusChem* **2013**, *6*, 1158–1162.
[3] S. De, S. Dutta, B. Saha, *ChemSusChem* **2012**, *5*, 1826–1833.
[4] *Encyclopedia of Applied Electrochemistry* (Eds.: G. Kreysa, K. Ota, R. F. Savinell), Springer New York, New York, NY, **2014**.
[5] S. De, B. Saha, R. Luque, *Bioresour. Technol.* **2015**, *178*, 108–118.
[6] I. Gandarias, P. L. Arias, J. Requies, M. El Doukkali, M. B. Güemez, *J. Catal.* **2011**, *282*, 237–247.
[7] Y. S. Yun, D. S. Park, J. Yi, *Catal. Sci. Technol.* **2014**, *4*, 3191–3202.
[8] R. Parsons, *Trans. Faraday Soc.* **1958**, *54*, 1053–1063.
[9] Z. Li, M. Garedew, C. H. Lam, J. E. Jackson, D. J. Miller, C. M. Saffron, *Green Chem.* **2012**, *14*, 2540–2549.
[10] P. Nilges, U. Schröder, *Energy Environ. Sci.* **2013**, *6*, 2925–2931.

[11] Z. Li, S. Kelkar, C. H. Lam, K. Luczek, J. E. Jackson, D. J. Miller, C. M. Saffron, *Electrochim. Acta* **2012**, *64*, 87 – 93.
[12] B. Mahdavi, A. Lafrance, A. Martel, J. Lessard, H. Me, L. Brossard, *J. Appl. Electrochem.* **1997**, *27*, 605 – 611.
[13] S. H. Pang, N. E. Love, J. W. Medlin, *J. Phys. Chem. Lett.* **2014**, *5*, 4110 – 4114.
[14] L. Chen, Y. Zhu, H. Zheng, C. Zhang, B. Zhang, Y. Li, *J. Mol. Catal. A* **2011**, *351*, 217 – 227.
[15] A. R. Ardiyanti, S. A. Khromova, R. H. Venderbosch, V. A. Yakovlev, I. V. Melián-Cabrera, H. J. Heeres, *Appl. Catal. A* **2012**, *449*, 121 – 130.
[16] M. Besson, P. Gallezot, *Catal. Today* **2003**, *81*, 547 – 559.
[17] I. Arends, R. A. Sheldon, *Appl. Catal. A* **2001**, *212*, 175 – 187.
[18] K. Manthiram, Y. Surendranath, A. P. Alivisatos, *J. Am. Chem. Soc.* **2014**, *136*, 7237 – 7240.
[19] *Metal Prices in the United States through 2010*: U.S. Geological Survey Scientific Investigations Report 2012 – 5188, U.S. Geological Survey, **2013**.
[20] K. Seto, A. Iannelli, B. Love, J. Lipkowski, *J. Electroanal. Chem. Interfacial Electrochem.* **1987**, *226*, 351 – 360.

Received: March 3, 2016
Revised: May 11, 2016
Published online on ■■ ■■, 0000

*K. J. Carroll, T. Burger, L. Langenegger, S. Chavez, S. T. Hunt, Y. Román-Leshkov, F. R. Brushett**

■■ – ■■

Electrocatalytic Hydrogenation of Oxygenates using Earth-Abundant Transition-Metal Nanoparticles under Mild Conditions

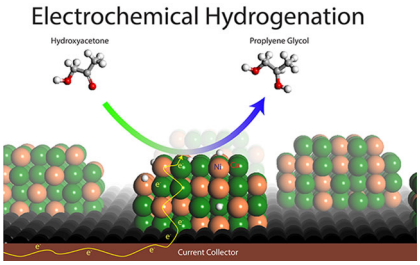

MITarbeiters of the Month: Electrocatalytic hydrogenation (ECH) is a sustainable pathway for the synthesis of value-added organic compounds, provided affordable catalysts with high activity, selectivity, and durability are developed. The performance of a series of copper, nickel, and copper–nickel nanoparticles on a carbon support towards ECH of hydroxyacetone is compared to that of ruthenium, platinum, and platinum–ruthenium nanoparticles. The non-precious metal electrocatalysts show promising conversion–time behavior, product selectivities, and Faradaic efficiencies.